CFD Analysis of Bed Textural Characteristics on TBR Behaviour: Kinetics, Scaling-up, Multiscale Analysis, and Wall Effects

Sebastián Uribe,[1] Mario E. Cordero,[1]* Luis G. Zárate,[1] José Javier Valencia López[2] and Reyna Natividad[3]

1. Departamento de Ingeniería, Universidad Popular Autónoma del Estado de Puebla, Pue., Puebla, México
2. Departamento de Procesos y Tecnología, Universidad Autónoma Metropolitana Cuajimalpa, Ciudad de México, México
3. Centro Conjunto de Investigación en Química Sustentable UAEM-UNAM, Toluca, Edo. de México, 50200, México

A simulation of a trickle bed reactor aided by computational fluid dynamics was implemented. With a Eulerian approach, geometrical characteristics were explicitly considered and two simultaneous heterogeneous reactions were included, hydrodesulphurization (HDS) and hydrodenitrogenation (HDN). This was performed in order to achieve the following: (1) attain further insight into a proper scaling-up procedure to be able to obtain the same hydrodynamics and kinetics behaviour in two reactors of different length and diameter scales; (2) develop a multiscale analysis regarding the communication of information between scales through the construction of a porous microstructure model from which the geometrical information of the microscale is captured by the effective transport coefficients (which affect the overall reactor behaviour); (3) investigate the effect of operation condition variations on hydrodynamics and kinetics; and (4) assess the deviations and further differences observed from average to punctual conversion values and the assumptions from kinetic literature models through a preliminary multiscale analysis.

The CFD results were validated against experimental pressure drop data as well as HDS and HDN conversion theoretical data. An excellent agreement was found. The model produces a significant improvement in hydrodynamic parameter prediction, achieving 5 times better accuracy in predicting pressure drops and 50 % improvement in holdup prediction. The fully coupled model predicts HDS conversion with 96 % accuracy and HDN conversion with 94 % accuracy. Results suggest that the best way to obtain similar kinetic and hydrodynamic behaviour in TBRs with different lengths and diameter length scales is by equaling the liquid holdup (ε_γ) or the mass velocities (L-G).

Keywords: TBR CFD simulation, hydrodesulphurization, scale-up/down process, multiscale-multiphysics approach

INTRODUCTION

In recent years, the requirement for optimization and improvement in many existing processes implemented in trickle bed reactors (TBR), such as hydrotreating processes, has increased as new requirements have been set by international regulations and norms.[1] These optimization tasks demand the reliable evaluation of hydrodynamic and kinetic key parameters, such as the holdup and pressure drop,[2–4] as well as the inclusion of geometrical heterogeneities, typical non-linearity of complex reaction mechanisms, essential characteristics and high coupling between reaction rates, and the mass transport and resistances to mass transfer between the three phases.[5–7] Such complexities have been the main focus in the study of hydrodesulphurization (HDS) processes and, despite the advances in their study, these still represent a great challenge to overcome.

In this sense, computational fluid dynamics (CFD) has become a reliable tool in the study of these systems that exhibit multiphysics multiscale nature with high nonlinearities and a high grade of coupling between the phenomena involved. CFD allows for taking into account the effect of the reactive conditions in the evaluation of the hydrodynamic key parameter, which represents an important advantage in contrast with the common experimental approach in which those parameters are evaluated in cold columns.[8] CFD also allows for access to the local scale phenomena that is hardly observed with experimental methods, such as the reaction rate inside the catalyst particles, local mass fluxes, and local concentration fields.

Despite the advances in understanding TBRs through CFD techniques, there are still challenges to surpass due to the great complexity of these systems and their highly coupled, multiphysics, multiscale, and multiphasic nature.[9] In this context, several efforts to improve the understanding of these systems have been developed from which two main kinds of contribution can be distinguished: 1) studies in which the hydrodynamic behaviour of the column is assessed (usually in the absence of mass transfer and reaction phenomena or with important simplifications in the multiphysics nature that allow the incorporation of more explicit descriptions of the bed textural characteristics[8,10–15]); and 2) works where the kinetic behaviour is studied, usually with important simplifications in the description of the void fraction of the bed (average equations) and that generally appeal to form factors to take into account the textural effects of the catalytic bed and effective transport coefficients. The simplicity of these works allows the incorporation of complex chemical reaction phenomena.[16–19]

Regarding the hydrodynamics studies that consider simplifications in the representations of the textural bed characteristics and the implementation of particular interfacial momentum exchange models (IMEM),[4,20–22] it can be seen that the current mathematical representation of the phenomena, and therefore the predictions of pressure drop, have significant deviations of up to 30 %. It can

* Author to whom correspondence may be addressed.
E-mail address: marioedgar.cordero@upaep.mx
Can. J. Chem. Eng. 9999:1–15, 2018

DOI 10.1002/cjce.23298
Published online in Wiley Online Library (wileyonlinelibrary.com).

be concluded that better descriptions of the distribution of the void fraction, due to the packing and geometry of the packing and the implementation of closures (IMEMs) that account for the gas-liquid, gas-solid, and liquid-solid interactions, are needed to improve the hydrodynamics behaviour predictions.[22–24] Therefore, the textural characteristics of the bed cannot simply be taken into account through form factors.[25,26]

Likewise, it has been observed that the hydrodynamic behaviour of TBRs has a remarkable effect on the maximum achieved conversions in the reactor.[6,27] There are important phenomena, such as liquid maldistribution, that affect the throughput of the TBR and they are mostly influenced by the size, shape, and packing of the catalyst particles.[6] Furthermore, the geometrical characteristics of the catalytic particles have been widely addressed by researchers and licensers in order to achieve greater contact surfaces that improve the efficiency in the reaction phenomena,[19,28] but the drawbacks in the hydrodynamic performance of the reactor have usually been neglected.

Regarding the modelling of HDS processes, important developments have been made in recent years with different approaches and assumptions; most contributions usually neglect the hydrodynamic behaviour and consider the solid phase effects, such as the catalyst shape and the distribution of the void phase, using form factors or empirical correlations.[29–31] In addition, it is common to find models in literature in which the kinetic behaviour of the TBR is addressed by considering plug flow models, yet overlooking the hydrodynamics behaviour of the reactor and, therefore, neglecting important transport phenomena as radial dispersion and the coupling with the two-phase hydrodynamics.[29,32,33] Furthermore, the effects of the intra-particle mass resistances in catalyst and the mass interchange between fluid-solid and gas-liquid phases are incorporated through effectiveness factors[29,33] and using a volumetric exchange term.

These kinds of models have been useful in assessing the overall kinetic behaviours of industrial-scale reactors and kinetic data in laboratory reactors; however, these models do not allow the evaluation of phenomena that affect the reactor throughput, such as liquid maldistribution. Moreover, the justification and support for the validity of the considered assumptions are never provided or, at least, not stated.

Recently, there have been contributions in the modelling of HDS processes with extended approaches, such as considering 3D simulations that couple the hydrodynamics with the mass transfer.[30,34] In this context, it is important to highlight the work of Silva et al.,[34] who developed a 3D CFD simulation that considers simultaneous HDS and hydrodearomatization (HDA), which allows the incorporation of radial dispersion and the coupling of the hydrodynamics. However, no validation for the hydrodynamic was presented and the effects of the bed textural characteristics were incorporated through a porosity distribution expression. This, implies that this CFD model does not distinguish between the three phases and suggests that the solid, gas, and liquid share the same domain.

Therefore, TBR studies with a more realistic representation of the geometry of the catalytic bed that consider coupling the hydrodynamics with the mass transport with reaction, and that use an IMEM that incorporates the three-phase interaction, are scarce and more studies are required. As far as the authors are concerned, there are no contributions in which such characteristics are coupled for an HDS process in a TBR and a punctual analysis of the local scale phenomena is analyzed.

The proposed heterogeneous CFD model in this work does the following: couples the two-phase hydrodynamics with the three-phase mass transport phenomena with reaction inside the solid phase for a hydrodesulphurization (HDS) process; incorporates the three-phase interaction through IMEM closures; and incorporates the textural bed characteristics through an explicit description of the fluid-solid interfacial areas $\left(A_{j\omega}\right)$ in a geometrical bed model in order to gain insight into the improvement of the reactor-scale behaviour predictions.

Another important aspect to note in the TBR CFD models is that multiscale analyses are scarce in literature, even though there have been important developments in establishing rigorous scaling procedures, such as the method of volume averaging. In this method, average (effective) equations for multiphase systems are obtained from valid local equations for each phase independently, which leads to expressions for effective transport coefficients. It is through these coefficients that the essential characteristics of the multiphysics nature is captured and the information regarding low scales phenomena is transported to upper scales.

It is important to mention that in the method of volume averaging, the values for effective transport coefficients and the validity of average transport equations have been proven[35] independently from each other. In addition, the effects of the multiphase and multiscale information captured by the transport coefficients at a lower length scale on the global behaviour of the system are almost never validated or proven.[35–37] Therefore, these tasks remain incomplete.

Analyses such as the one presented in this study represent an effort to quantitatively determine the magnitude of the influence of the down scales phenomena on upper scales. Here, the effect of the mass transport and reaction phenomena at catalyst scale is analysed in conjunction with the information of the geometrical porous microstructure at the catalytic particle (which is captured and scaled-up to the overall behaviour of the TBR through volume averaging method results of effective transport coefficients).

Another great challenge regarding the TBR performance is the lack of well-established scaling-up/down procedures based on scientific criteria. Historically, the scaling-up process from pilot to industrial reactors considers that physical phenomena remain unchanged at two different scale lengths, leading to an almost direct scaling process. Thus, the scaling-up in TBRs is based on equaling the liquid hourly space velocity (LHSV);[38] however, this equality involves lower pilot plant velocities from 10–100 times lower than industrial plants.[39] This causes a counterproductive effect on the mass transfer resistances and modifies the plug flow behaviour inside the reactor. In other words, the hydrodynamic behaviour between two reactors is different. In our previous work, we implemented a study comparing columns with different relations between length and diameter (L_R/D_R) and reactor diameter to pellet diameter ($N = D_R/d_P$). It was observed that to ensure a similar hydrodynamic behaviour inside two packed columns of different dimensions, the liquid holdups between both columns should be equalized.[22,40,41] This kind of equality, combined with a model that incorporates a rigorous description of the void fraction of the bed and considers an adequate closure for the interfacial momentum exchange model (IMEM), has led to predictions of pressure drops with an error that is down to 1.9 %,[22] which implies a 50 % improvement in holdup predictions and up to 5 times better accuracy in pressure drops. In this work, it is intended to extend such analysis to the mass transport in an HDS reactor.

In this work, a scale-up/down procedure aided by CFD techniques was investigated. In this procedure, the effect of the microscale phenomena, the three-phase interactions, and the

inclusion of the explicit textural characteristics were incorporated and their effect was perceived on the overall kinetic behaviour of the TBR. Finally, the effect of operation conditions is also evaluated. It is important to highlight that the mass transport includes simultaneous hydrodesulphurization (HDS) and hydrodenitrogenation (HDN) reactions that follow LHHW kinetics,[33] and that the complete model implies 13 mass transport equations, one per each species, 2 momentum transport equations for fluid phases, and three closures for the interactions between phases (IMEMs).

THEORY

Geometrical Model

A heterogeneous reactor model was developed in which both the interstitial and catalytic bed domains were built by improving a previously developed model for hydrodynamic studies.[22] The improved model consists of 24 layers of pellets with a total of 7323 catalytic particles and has a bed porosity of $\varepsilon_B = 0.41$. To avoid wall effects, there is a critical value (N_c) of the reactor to pellet diameters ratio ($N = D_R/d_p$) that must be considered in modelling these kinds of systems. With this in mind, it was previously observed that a value of $N \approx 9.1$ for hydrodynamics simulations and $N \approx 18$ in simulations coupling mass transport were adequate to neglect those effects.[24] It is important to note that these observations are in concordance with observed dimensions in experimental works, such as the works of Al-Dahhan and Dudukovic who had a value of $N = 20$.[23]

Further details regarding the bed configuration and construction of the geometrical model can be seen in Figure 1.

Momentum Transport Model

A Eulerian of two fluid phases approach was implemented, in which gas and liquid pseudo-phases were treated as interpenetrating, having the same domain (the interstitial domain), and having a volume average governing equation of continuity and momentum that was satisfied by each pseudo-phase. The volumes fractions (ε_i) are used to represent the space occupied by each phase and are constrained to satisfy $\sum_i \varepsilon_i = 1$. It is important to note that the solid pseudo-phase is explicitly considered by the geometry of the fixed bed, as depicted in Figure 1, and its interaction with the fluid pseudo-phases is considered with adequate boundary condition and the closure for the momentum interchange between the three pseudo-phases.

The continuity and momentum transport equations for the liquid ($j = \gamma$) and gas ($j = \beta$) pseudo-phases in a TBR that have been previously used by other researchers[42–44] are the following:

Hydrodynamic Model

$$\varepsilon_\gamma \rho_\gamma \nabla \cdot \mathbf{v}_\gamma = 0 \qquad (\rho_\gamma = cte) \tag{1}$$

$$\varepsilon_\beta \nabla \cdot (\rho_\beta \mathbf{v}_\beta) = 0 \tag{2}$$

$$\varepsilon_\gamma \rho_\gamma (\mathbf{v}_\gamma \cdot \nabla)\mathbf{v}_\gamma = \varepsilon_\gamma \nabla \cdot \left[-P\mathbf{I} + \mu_\gamma\left(\nabla \mathbf{v}_\gamma + (\nabla \mathbf{v}_\gamma)^T\right)\right] + \frac{\mathbf{F}_\gamma}{\varepsilon_\gamma} + \rho_\gamma \mathbf{g} \tag{3}$$

$$\varepsilon_\beta \rho_\beta (\mathbf{v}_\beta \cdot \nabla)\mathbf{v}_\beta = \varepsilon_\beta \nabla \cdot \left[-P\mathbf{I} + \mu_\beta\left(\nabla \mathbf{v}_\beta + (\nabla \mathbf{v}_\beta)^T\right) - \frac{2}{3}\mu_\beta(\nabla \cdot \mathbf{v}_\beta)\mathbf{I}\right] + \frac{\mathbf{F}_\beta}{\varepsilon_\beta} + \rho_\beta \mathbf{g} \tag{4}$$

Boundary Conditions

$$-\mathbf{n} \cdot \mathbf{v}_j = V_j^0 \quad (inlet) \tag{5}$$

$$\left[-P/\mathbf{I} + \mu\left(\nabla \mathbf{v}_j + (\nabla \mathbf{v}_j)^T\right)\right]\mathbf{n} = -\mathbf{n}P_0 \quad (outlet) \tag{6}$$

$$\mathbf{v}_j = 0 \quad (no\,slip,\ at\,fluid - solid\,interphase,\ A_{j\omega}) \tag{7}$$

Here ρ_i and μ_i are the scalar density and viscosity of each j-psuedo-phase, $\mathbf{v}_j$ is the interstitial velocity vector, $\mathbf{I}$ is the identity matrix, P is the pressure of gas and liquid phases, $\mathbf{g}$ is the gravitational acceleration, and $\mathbf{F}_j$ is the interaction force term between phases given by the following:

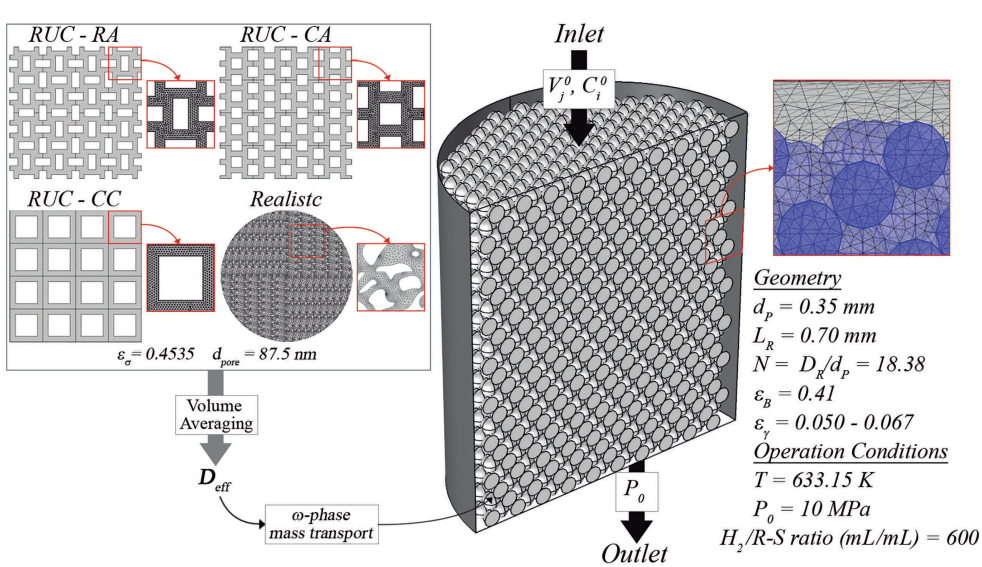

Figure 1. Details of the geometrical characteristics of the implemented CFD model.

$$\mathbf{F}_j = \sum_{j=1}^{n} K_{kj}(\mathbf{v}_k - \mathbf{v}_j) \tag{8}$$

Equation (8) is a closure term that describes the momentum exchange between solid (ω), liquid, and gas pseudo-phases, where the term $(\mathbf{v}_k - \mathbf{v}_j)$ is the slip velocity between phases k and j and K_{kj} is the momentum exchange coefficient that satisfies $K_{kj} = -K_{jk}$. To take into account the gas-liquid, gas-solid, and liquid-solid interactions, the Attou IMEM closure was selected since it seemed to be the most successful model to represent the interactions between phases.[22] It is important to remark that even though the Attou model is generally used to model the gas-solid interactions, this model was developed considering a complete wetting of the pellet and, thus, neglected the gas-solid interactions.[45] However, an extension of the Attou model for TBRs can be found in literature. It considers the gas-solid ($\beta - \omega$) interactions, which seems suitable and has led to appropriate hydrodynamics behaviour predictions with errors reported in literature down to 1.9 % in the pressure drop predictions.[22]

The Attou model is represented in Equation (9):

$$K_{\beta\gamma} = \varepsilon_\beta \left[\frac{E_1 \mu_\beta (1-\varepsilon_\beta)^2}{\varepsilon_\beta^2 d_p^2} \left(\frac{\varepsilon_\omega}{1-\varepsilon_\beta} \right)^{0.667} + \frac{E_2 \rho_\beta (\mathbf{v}_\beta - \mathbf{v}_\gamma)(1-\varepsilon_\beta)}{\varepsilon_\beta d_p} \left(\frac{\varepsilon_\omega}{1-\varepsilon_\beta} \right)^{0.333} \right]$$

$$K_{\beta\omega} = \varepsilon_\beta \left[\frac{E_1 \mu_\beta (1-\varepsilon_\beta)^2}{\varepsilon_\beta^2 d_p^2} \left(\frac{\varepsilon_\omega}{1-\varepsilon_\beta} \right)^{0.667} + \frac{E_2 \rho_\beta \mathbf{v}_\beta (1-\varepsilon_\beta)}{\varepsilon_\beta d_p} \left(\frac{\varepsilon_\omega}{1-\varepsilon_\beta} \right)^{0.333} \right]$$

$$K_{\gamma\omega} = \varepsilon_\gamma \left[\frac{E_1 \mu_\gamma \varepsilon_\omega^2}{\varepsilon_\gamma^2 d_p^2} + \frac{E_2 \rho_\gamma \mathbf{v}_\gamma \varepsilon_\omega}{\varepsilon_\gamma d_p} \right] \tag{9}$$

where E_1 and E_2 are the first and second Ergun constant respectively (taken from Al-Dahhan and Dudukovic[2]).

It is noteworthy that the Attou model was developed from theoretical considerations by deriving a balance of force based on the macroscopic laws of mass and momentum. One of the advantageous characteristics of this model, in contrast to empirical models or relative permeability models, is that this model lacks adjustable constants. In addition, the model was developed explicitly for a trickle regime based on the Kozeni-Carman equation and incorporates the physical properties, the superficial velocity of the liquid, the void fraction of the bed, and the tortuosity of the bed, assuming these as inversely proportional to the volume fraction of the bed. The prediction of the hydrodynamic parameters by the model falls in the range of error shown by other correlations and the experimental data of pressure gradient and liquid saturation.

Mass Transport Model

The mass transport model is constituted by convection-diffusion transport in gas and liquid pseudo-phases and diffusion-reaction in the solid phase. Three pseudo-phases have been considered: two fluid pseudo-phases (one liquid phase and one gas phase), by virtue that these share the same domain; and one solid pseudo-phase, which is a pseudo-phase because the catalysts are actually constituted by a solid matrix ($\sigma - phase$) and a fluid domain ($\lambda - phase$) that fills the interstitial space left by the solid (which implies that the catalyst is completely wet). The average mass transport model described by Equations (10)–(17), considers the mass exchange between gas-liquid-solid phases as a boundary condition if the interphase area is known and as a volumetric term in the mass transport equation if this area is unknown.

The following is the gas phase mass transport equation:

$$\nabla \cdot \left(-D_i^\beta \nabla \langle C_i^\beta \rangle \right) + \mathbf{v}_\beta \cdot \nabla \langle C_i^\beta \rangle = N_i^{\beta\gamma} / \varepsilon_\beta \quad (i = H_2, H_2S, NH_3) \tag{10}$$

The following are the boundary conditions set for the gas phase mass trasport:

$$\langle C_{H_2}^\beta \rangle = C_{H_2}^0; \quad \langle C_{H_2S}^\beta \rangle = \langle C_{NH_3}^\beta \rangle = 0 \quad (inlet) \tag{11}$$

$$-\mathbf{n} \cdot D_i^\beta \nabla \langle C_i^\beta \rangle = 0 \quad (outlet) \tag{12}$$

$$-\mathbf{n} \cdot D_i^\beta \nabla \langle C_i^\beta \rangle + \mathbf{v}_\beta \langle C_i^\beta \rangle = 0 \quad (gas - solid\, interphase,\ A_{\beta\omega}) \tag{13}$$

The following is the liquid phase mass transport equation:

$$\nabla \cdot \left(-D_i^\gamma \nabla \langle C_i^\gamma \rangle \right) + \mathbf{v}_\gamma \cdot \nabla \langle C_i^\gamma \rangle = N_i^{\gamma\beta} / \varepsilon_y \quad (i = H_2,\ H_2S,\ NH_3,\ R-S,\ R-N) \tag{14}$$

The following are the boundary conditions set to the liquid phase mass transport:

$$\langle C_{R-S}^\gamma \rangle = C_{R-S}^0;\ \langle C_{R-N}^\gamma \rangle = C_{R-N}^0;\ \langle C_{H_2}^\gamma \rangle = \langle C_{H_2S}^\gamma \rangle = \langle C_{NH_3}^\gamma \rangle = 0 \quad (inlet) \tag{15}$$

$$-\mathbf{n} \cdot D_i^\gamma \nabla \langle C_i^\gamma \rangle = 0 \quad (outlet) \tag{16}$$

$$-\mathbf{n} \cdot D_i^\beta \nabla \langle C_i^\beta \rangle + \mathbf{v}_\beta \langle C_i^\beta \rangle = -D_{eff,i} \nabla \langle C_i^\omega \rangle^\omega \quad (liquid - solid\, interphase,\ A_{\gamma\omega}) \tag{17}$$

In the equations above, $\langle C_i^\beta \rangle$ and $\langle C_i^\gamma \rangle$ are the average concentration for each i-species in the gas and liquid pseudo-phases, respectively. The average volumetric mass exchange between gas and liquid for the i-species is given as $N_i^{\beta\gamma} = K_{g,i}^{\beta\gamma} \left(\langle C_i^\beta \rangle R_g T / H_i - \langle C_i^\gamma \rangle \right)$ and it is satisfied that $N_i^{\beta\gamma} = -N_i^{\gamma\beta}$. Here R_g is the constant of ideal gases, T the operating temperature, and $K_{g,i}^{\beta\gamma}$ and H_i are the gas-liquid convective mass transfer coefficient and the Henry coefficient for the i-species, respectively.

The following is the solid phase mass transport equation:

$$\nabla \cdot \left(-\varepsilon_\lambda \mathbf{D}_{eff,i}^\omega \nabla \langle C_i^\omega \rangle^\omega \right) = v_i \langle r_q^\omega \rangle^\omega \quad (i = H_2,\ H_2S,\ R-S,\ R-N,\ NH_3;\ q = HDS,\ HDN) \tag{18}$$

The following are the boundary conditions set to the solid phase mass transport:

$$\langle C_i^\omega \rangle^\omega = \langle C_i^\gamma \rangle \quad (liquid - solid\, interphase,\ A_{\gamma\omega}) \tag{19}$$

Table 1. Physical properties at reaction conditions used in the CFD model

ρ_γ	705.9 kg/m^3	$D^\gamma_{H_2S}$	1.10×10^{-8} m^2/s	H_{NH_3}	44 450.2 Pa m^3/mol
μ_γ	2.969×10^{-9} Pa s	$D^\gamma_{H_2}$	1.33×10^{-8} m^2/s	H_{H_2}	17 676 Pa m^3/mol
ρ_β	3.79 kg/m^3	$D^\gamma_{NH_3}$	1.003×10^{-9} m^2/s	$K^{\beta\gamma}_{H_2S}$	6.29×10^{-2} 1/s
μ_β	1.47×10^{-5} Pa s	$D^\beta_{H_2S}$	2.37×10^{-6} m^2/s	$K^{\beta\gamma}_{H_2}$	5.72×10^{-2} 1/s
$-\Delta H_{HDS}$	251 548 J/mol	$D^\beta_{H_2}$	1.79×10^{-8} m^2/s	$K^{\beta\gamma}_{NH_3}$	0.2081 1/s
MW_{gasoil}	319.98 g/mol	$D^\beta_{NH_3}$	2.3×10^{-6} m^2/s	$K^{\gamma\omega}_{H_2S}$	8.464×10^{-6} m/s
D^γ_{R-S}	3.25×10^{-9} m^2/s	H_{H_2S}	214 673 Pa m^3/mol	$K^{\gamma\omega}_{NH_3}$	1.204×10^{-6} m/s

In the case of the solid domain, the averaged mass transport equations consider diffusive transport and generation due to the reaction, as shown in Equation (18), which is satisfied in the catalyst domain.[46,47]

In Equation (18), $\langle C_i^\omega \rangle^\omega$ is the average concentration in the solid pseudo-phase (ω), v_i is the stoichiometric coefficient, and $\langle r_q^\omega \rangle^\omega$ are the volumetric reaction rates for both HDS and HDN that are given in Equations (22) and (23).

$\mathbf{D}^\omega_{eff,i}$ are the effective diffusivity for each species that was evaluated in a previous work,[48] in which the effect of the quantity of details of geometrical characteristics of the porous matrix microstructure was evaluated.

Physical Properties

The physical properties of the sulphurated light gasoil (R-S and R-N) and the H_2, NH_3, H_2S species, as well as the kinetic parameters and mass transport properties were calculated with the reported expressions and correlations found in literature.[22,23,29,49–51] Table 1 shows the physical properties, input to the model.

Kinetic Model

Due the presence of a large number of sulphur compounds in the light gasoil, determining their concentrations and properties is quite a demanding task and, therefore, to rigorously consider all sulphur compounds in the model is a further challenge. Then, the gasoil is treated as a pseudo-component that satisfies the following stoichiometric relation:

$$v_{r-s}R - S_{(liq)} + v_{H_{2,1}}H_{2(g)} \rightarrow v_{R-H_2}R - H_{2(liq)} + v_{H_2S}H_2S_{(g)} \tag{20}$$

$$v_{R-N}R - N_{(liq)} + v_{H_{2,2}}H_{2(g)} \rightarrow v_{R-H_3}R - H_{3(liq)} + v_{NH_3}NH_{3(g)} \tag{21}$$

where $v_{R-S} = -1, v_{H_{2,1}} = -2$, $v_{R-H_2} = 1, v_{H_2S} = 1$, $v_{R-N} = -1$, $v_{H_{2,2}} = -3$, $v_{R-H_3} = 1$, and $v_{NH_3} = 1$. The kinetic expression used here is shown in Equations (22) and (23) and was proposed by Chacón et al.[33] (this expression considers a bimolecular reaction that has the same probability to be adsorbed on the catalyst):

$$-\langle r^\omega_{HDS} \rangle^\omega = \frac{k_{HDS}\langle C^\omega_{RS} \rangle^\omega \left(\langle C^\omega_{H_2} \rangle^\omega \right)^{0.5}}{\left(1 + K_{H_2S}\langle C^\omega_{H_2S} \rangle^\omega\right)^2} \tag{22}$$

$$-\langle r^\omega_{HDN} \rangle^\omega = \frac{k_{HDN}\langle C^\omega_{RN} \rangle^\omega \langle C^\omega_{H_2} \rangle^\omega}{\left(1 + K_{NH_3}\langle C^\omega_{NH_3} \rangle^\omega\right)^2} \tag{23}$$

The reaction rate constants for the HDS and HDN reactions and the adsorption constants for H_2S and NH_3 are given by Equations (24) and (25), respectively:

$$k_{HDS}\left[\frac{(m^3)_{0.5}}{mol}/s\right] = k^0_{HDS}e^{(-E_{HDS}/R_gT)}$$
$$k_{H_2S}\left[m^3/mol\right] = k^0_{H_2S}e^{(-Q_{H_2S}/R_gT)} \tag{24}$$

$$k_{HDN}\left[m^3/mol \cdot s\right] = k^0_{HDN}e^{(-E_{HDN}/R_gT)}$$
$$k_{NH_3}\left[m^3/mol\right] = k^0_{NH_3}e^{(-Q_{NH_3}/R_gT)} \tag{25}$$

Other kinetics parameters are shown in Table 2.

The kinetic model using these parameters conducted to relative errors of 3.25 % and 3.98 % for HDS and HDN conversion when compared with experimental values[41] (which had the highest error margin of 0.3 wt%[32]).

Effect of Catalyst Porous Geometry

The effect of the geometry of the catalyst's porous microstructure and its geometrical representation over the concentration and conversion fields in the overall TBR was studied in order to perform a multiscale analysis involving micropores, catalyst, and reactor length scales. This was performed through the application of the method of volume averaging results found in literature.[35] This method allowed us to obtain the effective mass transport equations valid in all the pseudo-homogeneous catalyst domains from the local equations valid in the interstitial fluid domain ($\lambda - phase$) inside the porous microstructure of the catalyst. It is important to highlight that in the porous microstructure of the catalyst, the chemical reaction phenomena take place in the interfacial area inside the pores $A_{\lambda\sigma}$.[35]

In the process of obtaining average equations, the main steps are to use the average operator $\langle C_i^j \rangle = \frac{1}{V}\int_{V_\lambda} C_i^j\, dV$ and apply it to the local equations. Then, integral theorems such as the mean or divergence, average theorems, and Gray's decomposition of scales $C_i^j = \langle C_i^j \rangle^j + \tilde{C}_i^j$ are used and an analysis of the magnitude of scales is performed in order to remove local variables. Due to the decomposition of scales, terms of deviation of average quantities remain and, therefore, a closure is used to obtain a closed average equation and allow the evaluation of the effective coefficients.

As previously mentioned, the method of volume averaging also provides expressions to evaluate the effective transport coefficients that appear in average equations.[35] In this case, the effective diffusivity ($\mathbf{D}_{eff}$) is evaluated by the following expression:

Table 2. Kinetic parameters for HDS and HDN reactions

$k^0_{HDS}\left[\left(\frac{m^3}{mol}\right)^{0.5}/s\right] = 6.46125 \times 10^{-5}$	$k^0_{HDN}\left[m^3/mol \cdot s\right] = 3.26268$
$E_{HDS}[J/mol] = 90\,180$	$E_{HDN}[J/mol] = 80\,680$
$k^0_{H_2S}\left[m^3/mol\right] = 0.038$	$k^0_{NH_3}\left[m^3/mol\right] = 2.55 \times 10^{11}$
$Q_{H_2S}[J/mol] = 2\,530$	$Q_{NH_3}[J/mol] = 111\,000$

$$\mathbf{D}_{eff} = D_\gamma \left(\mathbf{I} + \frac{1}{V_\lambda} \int_{A_{\lambda\sigma}} \mathbf{n}_{\lambda\sigma} \mathbf{b}_\lambda dA \right) \tag{26}$$

To evaluate the effective transport coefficient, it is necessary to solve the boundary value problem for closure vector $\mathbf{b}_\lambda$, as shown in Equations (27)–(29) (in which Equation (27) is the closure vector and Equations (28) and (29) are boundary conditions):

$$\nabla^2 \mathbf{b}_\lambda = 0 \tag{27}$$

$$-\mathbf{n}_{\lambda\sigma} \cdot \nabla \mathbf{b}_\lambda = \mathbf{n}_{\lambda\sigma} \quad (liquid - solid\ interphase\ inside\ catalysts,\ A_{\lambda\sigma}) \tag{28}$$

$$\mathbf{b}_\lambda(\mathbf{r} + l_i) = \mathbf{b}_\lambda(\mathbf{r}) \quad (for\ i = 1,\ 2,\ 3\ \ldots) \tag{29}$$

It is important to highlight that, to a certain extent, the closure vector captures the essential geometrical characteristics of the interface between the solid (σ) and fluid (λ) phases inside the pores. This geometric information is then transported to the coefficient of effective diffusivity by the closure vector in Equation (26), which is then valid and used in the mass transport equation for the solid pseudo-phase, as shown in Equation (18).

This represents a multiscale analysis that involves the study of phenomena at porous length scale, pellet length scale, and reactor length scale and allows the quantification of information that goes from one scale to another.

Regarding this last point, in an effort to quantify the effect of the microstructure geometrical information that is captured in the effective diffusivity coefficient over the TBR kinetic behaviour, different diffusivity values coming from different geometrical representations of the porous matrix and its superficial areas were tested (which are depicted in Figure 1). Four representative geometrical models to emulate the porous microstructure were set, and their effect over the HDS and HDN reactions conversion was observed. Further details of the evaluation of the effective diffusivity in those regions is presented elsewhere,[48] and a summary of the obtained effective coefficient values and details of geometrical microstructure representation can be seen in Table 3, in addition to other values that have been reported in literature.

In all of these cases, the same porosity of the porous media representation was established (ε_γ), which is within the common range for a porous catalyst for an HDS process.

It is noteworthy that the solution of the closure vector field ($\mathbf{b}$) is usually obtained in a periodic representative unitary cell (RUC), such as the CC, CA, and RA models, which are simplified representations that are assumed to capture the geometrical characteristics of the porous media. The evaluation of the closure vector field in the proposed realistic model (RM) in this work is the only reported work in which the intricate geometry of the porous media is represented and the geometrical complexities of the microstructure are explicitly considered.

Table 3. Effective diffusivities evaluated from the micropores representations and literature models

Representation	$\mathbf{D}_{eff,xx}/D\gamma$	*Literature model*	$D_{eff}/D\gamma$
CC	0.3602	Maxwell (M)	0.4455
CA	0.3361	Weisberg (W)	0.4197
RA	0.3275	Smith (S)	0.2987
Realistic (RM)	0.2228		

Note: $\mathbf{D}_{eff,xx}/D_\gamma \approx \mathbf{D}_{eff,yy}/D_\gamma$

Scaling-Up

To gain an insight into the scaling-up of the TBR, four cases were established to compare a model with different reactor length to reactor diameter ratios (L_R/D_R) and different N values, to the model proposed by Chacón et al. These four cases were established by either matching the models' liquid and gas hourly space velocities (*LHSV-GHSV*), liquid and gas mass velocities (*L-G*), Reynolds number $(Re^\gamma - Re^\beta)$, or liquid holdup $(\varepsilon_\gamma - \varepsilon_\beta)$ with those of the model proposed by Chacón et al.[33] It is important to note that due to the difference in lengths, two or more of these parameters cannot be matched at the same time.

The first step in the comparison process was that from the LHSV and the feed H_2/gasoil volume ratio considered by Chacón, the geometrical characteristics of their reactor, and the physical properties of the species, the following were calculated: the liquid and gas mass velocities (L, G); Reynolds number $(Re^\gamma - Re^\beta)$; liquid holdup$(\varepsilon_\gamma, \varepsilon_\beta)$; and liquid and gas velocities (v_γ, v_β). Then, the selected parameter for the comparison cases was equalized in the CFD model, generating the four aforementioned cases.

Details of the geometrical characteristics of the model and the inlet hydrodynamic parameters in the comparison cases can be seen in Table 4.

Computation

All of the models were implemented in COMSOL Multiphysics 5.3, in a Dell Precision workstation equipped with a dual socket Intel® Xeon® E5-2603 v3 processor and 160 GB of RAM memory. The implemented solver was a parallel direct sparse solver (PARDISO) with a segregated approach to improve the convergence of the multiphysic problem.

Analyses regarding the mesh dependency were conducted in order to neglect meshing effects over the results fields, taking as criteria the average velocity at the reactor outlet, pressure drop, and concentration fields for the TBR model and taking as criteria the evaluated effective diffusivity value for each porous microstructure model.

The TBR cases were 3D CFD simulations, for which a tetrahedral elements mesh of up to 2.7×10^6 elements was implemented, while the porous microstructure models were 2D CFD simulations, for which a triangular elements mesh of up to 3.6×10^6 elements was applied. Details of the mesh (see Figure 1), consumed RAM memory, and computing times can be seen in Table 5.

Model Assumptions

The CFD model that was built considers that the reactor operates in a low interaction trickle regime where the gas and liquid flow co-currently. Due to the reactor's small dimensions ($L_R \approx 0.7$ cm, $D_R \approx 0.64$ cm), the temperature gradients are expected to be very small and it can be assumed that the reactor operates isothermally. As a result, the pressure gradient is very small ($\Delta P \approx 20$ Pa) and the density and viscosity of gas and liquid phases are considered constant. Also, it was assumed that the catalyst activity does not change with time and that vapourization and condensation of the gasoil does not take place. Chemical reactions take place only inside the solid catalyst, which is considered to be completely wet, for purposes of the mass transport model.

Regarding the geometrical details of the packed bed, the ordered packing of the catalyst particles is considered to capture enough information about the distribution of the void fraction (also, the N value is considered as sufficient to neglect the wall effects) and it is possible to model only half of the reactor domain by means of a symmetry condition set in a middle axial cut plane. It is important

Table 4. Geometrical characteristics and inlet conditions of the comparison cases

		Comparison case			
	Chacón et al.[33]	LHSV-GHSV	L-G	Re^{γ}-Re^{β}	$\varepsilon_{\gamma} - \varepsilon_{\beta}$
Geometry					
L_R (cm)	12	0.70	0.70	0.70	0.70
D_R (cm)	1	0.64	0.64	0.64	0.64
N	28.57	18.38	18.38	18.38	18.38
Inlet conditions					
C^0_{R-S} (mol/m^3)	54.8078	54.8078	54.8078	54.8078	54.8078
C^0_{R-N} (mol/m^3)	8.82	8.82	8.82	8.82	8.82
$C^0_{H_2}$ (mol/m^3)	1930.2	1930.2	1930.2	1930.2	1930.2
LHSV [1/h]	0.00 028	0.00 028	0.0048	0.0074	0.0049
GHSV (1/h)	0.1667	0.1667	2.8608	4.4465	2.9651
L (kg/m^{2}s)	0.0235	0.0013	0.0235	0.0366	0.0244
G (kg/m^{2}s)	0.0758	0.0044	0.0758	0.1178	0.0786
Re^{γ}	0.7922	0.0297	0.5097	0.7922	0.5283
Re^{β}	51.5665	1.9329	51.5665	34.9868	
ε_{γ}	0.06 902	0.03 525	0.03 525	0.06 902	

Table 5. Details of the computational resources required in the CFD models

Model	Mesh (elements)	RAM memory (GB)	Computing time
Closure vector	3.6×10^6	13.4	0.3 h
TBR	2.7×10^6	120	3 h – 1 week*

*Depending on the tested case

to highlight that since the geometrical model explicitly considers the variations of the void fraction, there is no need to include an expression to model such variation across the reactor. Further discussion regarding the validity of these assumptions has been presented in previous work,[9,22] in which the considered criteria as well as the predicted results supported the assumptions.

RESULTS AND DISCUSSION

Figure 2a shows the average conversion fields for the HDS and HDN reactions along the reactor length using the four comparison methods, a procedure that was briefly discussed in the "Scaling-Up" section and that was previously discussed.[22] Figure 2a also shows the conversion fields for those reactions reported by Chacón et al.[33] for comparison purposes. Figure 2b shows the average concentration fields for the sulphurated (R-S) and nitrated (R-N) species for the same cases as Figure 2a.

When comparing the sulphurated and nitrated species conversions ($X_{R\text{-}S}$ and $X_{R\text{-}N}$) predicted by the CFD model with the theoretical data from Chacón et al.,[33] the best predictions are achieved when the holdup $(\varepsilon_{\gamma}, \varepsilon_{\beta})$ or the liquid and gas mass velocities (L-G) are equalized. The deviations obtained are 3.77 and 5.12 %, respectively for the R-S outlet conversion and 6.05 and 7.64 %, respectively for the R-N at the TBR outlet conversion.

It should be kept in consideration that the model used to compare concentrations and conversions corresponds to an effective medium model (plug flow model), where the fluid phases share domain; so, the concentrations and conversions obtained in those models correspond to average quantities. In addition, the Chacón et al. model conducted errors of 3.25 and 3.98 % for HDS and HDN conversion[33] when compared with the experimental data from Botchwey et al.[32]

A comparison between the calculated errors in the predictions of the average TBR outlet conversion for the HDS and HDN reactions with the corresponding data of Chacón et al.'s system

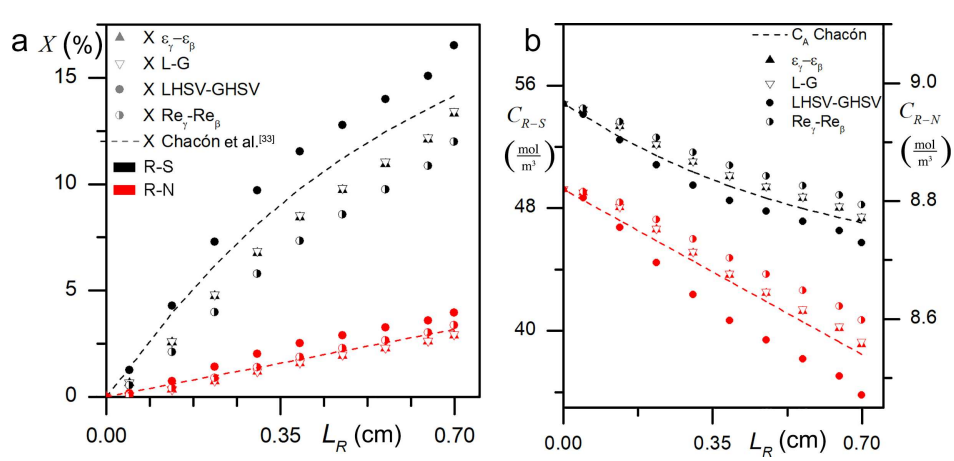

Figure 2. (a) HDS and HDN average reaction conversion fields using the four comparison methods for two columns with different dimensions; and (b) R-S and R-N average concentration fields using the four comparison methods for two columns with different dimensions.

at the same length of our model can be seen in Figure 3a. Also, Figure 3b shows the mean absolute relative errors (MARE) in the prediction of dimensionless pressure drops (Ψ) when compared with the experimental data provided by Al-Dahhan and Dudukovic[23] in the hydrodynamic model that has been presented in a previous work.[22] Figure 3c shows the parity plots corresponding to the validation of the pressure drop and liquid phase holdup predictions for the CFD model against the experimental data of Al-Dahhan and Dudukovic[23] for the case of high pressure operation (P = 3.55 MPa) and for the four cases implemented to compare both columns. It can be seen that for both hydrodynamics and kinetics tests, the lowest deviations in the prediction of pressure drops and conversions ($X_{R\text{-}S}$, $X_{R\text{-}N}$, Ψ at P = 0.31 MPa and Ψ at P = 3.55 MPa) are exhibited when equaling the holdup $(\varepsilon_\gamma - \varepsilon_\beta)$ or the liquid and gas mass velocities (*L-G*) in both systems. The largest deviations were obtained equaling the liquid and gas hourly space velocities (*LHSV-GHSV*), or the Reynolds numbers (Re^γ, Re^β), with errors of up to 90 % in the pressure drop predictions and 25 % in the conversion predictions. It is worth noticing that equaling *LHSV-GHSV* is currently the most applied criterion for the scaling-up of TBRs.[38]

The results shown in Figures 2 and 3 also allow us to infer that, for the tested cases, the way to obtain similar kinetic behaviours in two columns with different dimensions is also by equalizing the holdup $(\varepsilon_\gamma - \varepsilon_\beta)$ or the liquid and gas mass velocities (*L-G*). Therefore, when the liquid holdup or the mass velocities are equalized in two systems of different L_R/D_R and N values, a similar hydrodynamic and kinetic behaviour is expected to be achieved. These results suggest a possible scale-up procedure based on the hydrodynamics analysis of the systems; however, this needs to be confirmed for other systems.

In order to gain insight into the scaling-up of the effects of the catalyst pore microstructure representation and to quantify the effect of its geometrical characteristics over the kinetic behaviour at reactor scale, the cases presented in Table 3 were assessed. The information of these representations is captured by the evaluated effective diffusivity coefficient in each of them. The effect of these is shown in Figure 4a–d.

Figure 4a shows the components of the $\mathbf{b}_\lambda$ vector field evaluated in the realistic representation model and Figure 4b shows the differences in the prediction of the R-S average concentration fields in a region close to the reactor model's outlet, obtained with the different geometrical representations of the microstructure and by literature models. Cases with different geometrical representations of the microstructure were tested for both comparison cases $\varepsilon_\gamma - \varepsilon_\beta$ and *L-G*, which had led to the most consistency in both hydrodynamic parameters and conversions. From this, it can be seen that the geometrical differences in the representation of the microstructure can lead to differences in predictions of the concentration fields at a reactor scale with errors of up to 29.97 %. Similar observations can be made about Figure 4c and d, which show the average R-S and R-N concentration field through the whole reactor length, respectively, as well as the relative errors found within different cases of CFD simulations in other literature.[33]

It is worth noting that the proposed microstructure representations that led to the most similarity in the prediction of the R-S kinetic behaviour to data found in literature (RUC-CC) have an effective diffusivity coefficient that differs in a 38.15 % from the case (RM) that had the least similarity in the predictions. This led to differences of 23.08 % of R-S conversion and 30.59 % for R-N conversions between them.

Similar observations can be made about the other microstructure representation cases tested and the literature models that were considered. Figure 5 shows details about the effect of the geometrical representation of the microstructure of the catalyst particle over average R-S and R-N conversions at the reactor outlet. It uses RUC-CC as a reference case for comparison purposes.

These results suggest that the predicted kinetic behaviour at reactor scale is significantly sensitive to the changes in the representation of the porous microstructure geometrical characteristics and that there seems to be an inverse proportionality from the effective diffusivity coefficient deviation to the deviation in the prediction of the HDS and HDN reaction conversions; for example, if the effective diffusivity varies in 23 % (RM case), the R-S and R-N conversion varies in −10.1 % and −12.65 %.

Also, from Figure 5, it can be seen that the model that considers more intricate geometrical details, such as the anisotropies of the porous media and important variations in tortuosity and restriction factors (RM), leads to the greatest errors in R-S and R-N conversion predictions. Models that consider simpler geometrical details and an isotropic media, such as CC, RA, and CA, lead to the best predictions even though these last models do not consider actual properties of the porous media. To explain such observations, it must be considered that the reactor that is used to experimentally determine expressions of the reaction rate is of very small dimensions and was set for isothermal operation. In

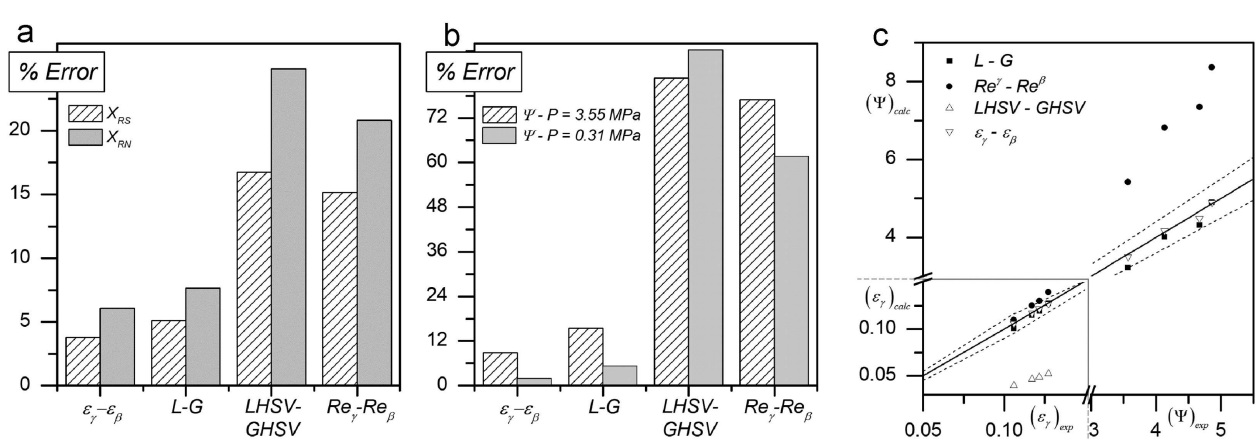

Figure 3. (a) HDS and HDN average reaction conversion fields using the four comparison methods for two columns with different dimensions; (b) mean average absolute errors in the predictions of dimensionless pressure drops at two different operation pressures using the four comparison methods for two columns with different dimensions; and (c) parity plot of the predicted holdup and dimensionless pressure drop by the model and experimental data.

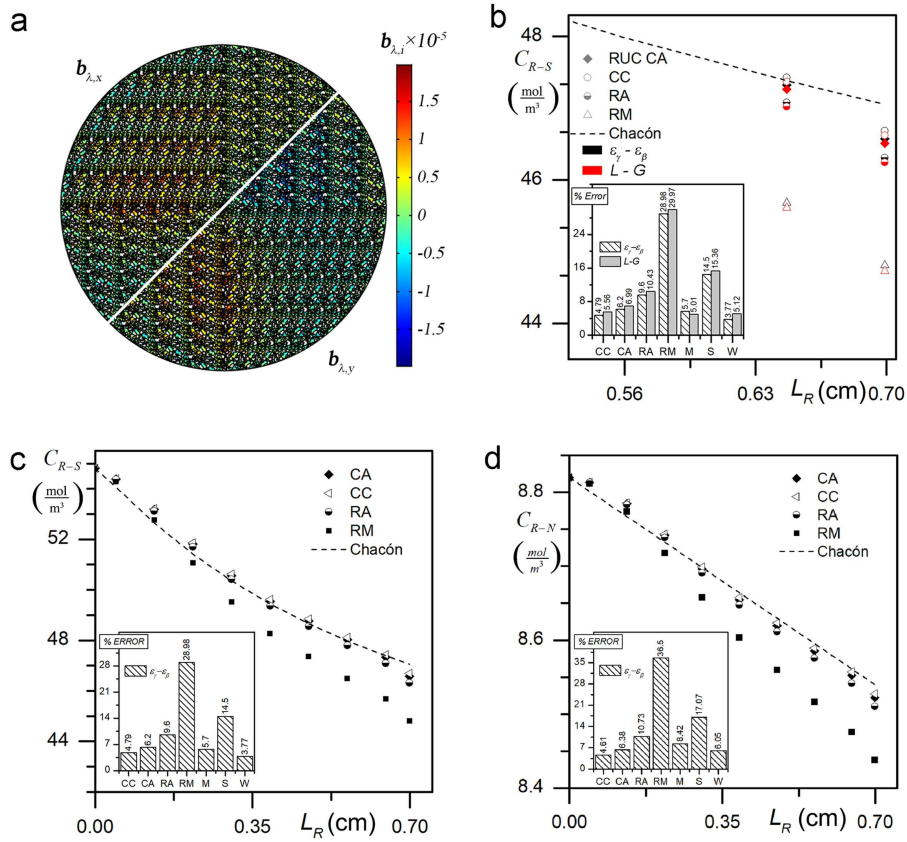

Figure 4. (a) Closure vector (**b**) field components evaluated in the realistic model representation; (b) average R-S concentration in a zoomed in region close to the reactor outlet, predicted with the different microstructure representations, for $\varepsilon_\gamma - \varepsilon_\beta$ and L-G comparison cases; (c) average R-S concentration field along the reactor model predicted by the different microstructure representations; and (d) average R-N concentration field along the reactor model predicted by the different microstructure representations.

addition, the reactor operated in a plug flow, and a small diameter of the catalytic particles (practically a powder) were selected in order to minimize the diffusional effects inside the catalyst.

Regarding the catalyst shape and size, it is expected that the nature of the microstructure of a catalyst in powder form is substantially different from an extruded catalyst. For example, the anisotropic nature is expected to be greater in the extruded catalyst than in the powder. This could be the reason why simplified isotropic geometries are better aligned with experimental conversion data from an experimental reactor with the aforementioned characteristics. Another possible explanation could be that there are important unconsidered deviations from plug flow in the experimental and theoretical reactors that were used to compare as opposed to a more adequate representation of an isotropic geometry using a simplified geometric representation of the microstructure.

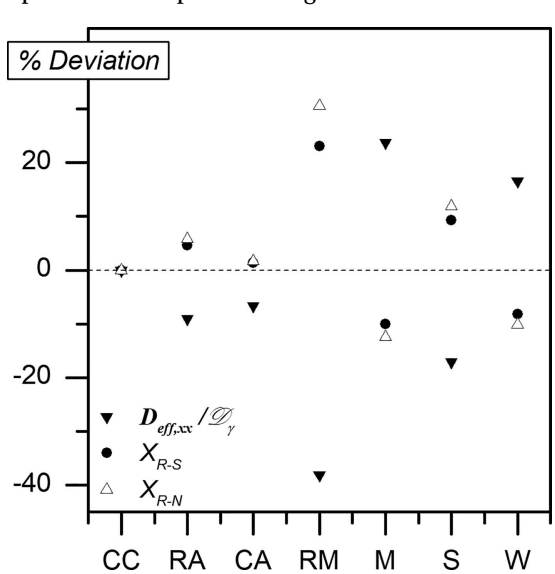

Figure 5. Deviations of the effective diffusivity, and HDS and HDN reaction conversions from the CC model base case.

Another aspect of interest in this work is the evaluation of the effect of the operating conditions in the TBR on both the hydrodynamic and kinetic behaviour of the HDS process. In this regard, as was already mentioned, studies in which the effect of the gas and liquid phases feed velocities on the hydrodynamic behaviour is analyzed can be found in literature, as well as studies where the effect of the pressure and temperature on the conversion obtained in the HDS reactor is analyzed. In such studies, however, the effect of hydrodynamics (pressure drop and holdup), and its coupled nature with the mass-reaction phenomena, is neglected. In fact, this simplification is assumed in the work that was used to compare the conversion values.[33]

The analysis of the operating conditions with the present CFD model is important because it considers the effect of hydrodynamics over the kinetic behaviour of the reactor and vice versa, which is somewhat closer to what happens in an actual HDS reactor. This also allows us to investigate phenomena that other models ignore.

Regarding the analysis of the operating conditions, taking as a base case the $\varepsilon_\gamma - \varepsilon_\beta$ case, four cases were established by increasing (+) or decreasing (−) the liquid or gas mass velocities:

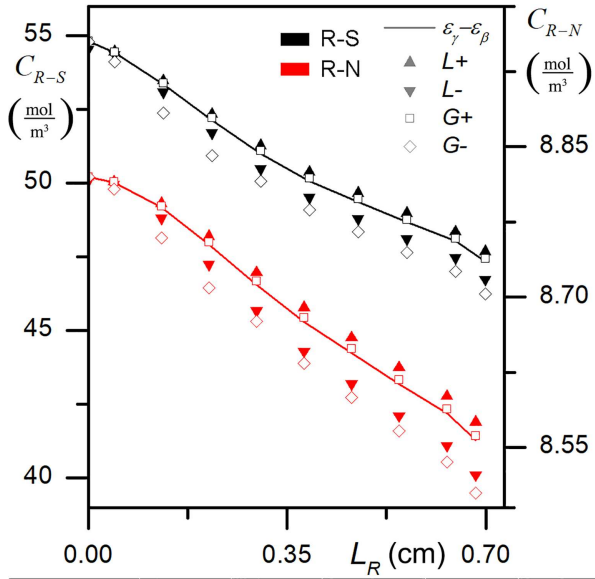

	$\varepsilon_\gamma - \varepsilon_\beta$	L+	L-	G+	G-
X_{RS}	0.136	0.13	0.147	0.134	0.156
X_{RN}	0.029	0.027	0.033	0.029	0.035
ε_γ	0.069	0.078	0.046	0.066	0.073
LHSV (1/s)	0.004	0.008	9E-4	0.004	0.004
GHSV (1/s)	2.965	2.965	2.965	5.149	0.572
$LHSV^{-1}$ (s)	202.3	112.4	1011.	202.3	202.3
$GHSV^{-1}$ (s)	0.337	0.337	0.337	0.194	1.747

Figure 6. Effect of varying the liquid and gas mass velocities over R-S and R-N average concentration field along the reactor.

1) L+, G (L+ case); 2) L−, G (L− case); 3) L, G+ (G+ case); and 4) L, G− (G− case).

The effect of such variations over the sulphurized and nitrated species average concentration along the reactor length can be seen in Figure 6.

For both nitrated and sulphurated species, when liquid or gas mass velocities increase (L+ and G+ cases), the conversion decreases, and when the liquid or gas mass velocity decreases, (L− and G− cases) the conversion increases. Moreover, the effect of varying liquid mass velocity over the kinetic behaviour of TBR is more pronounced than that of varying the gas mass velocity. It is important to keep in mind that the gas and liquid mass velocities are related to liquid and gas phase distribution inside the TBR, the liquid and gas residence time, the space velocity, and finally over its kinetic behaviour.

In Figure 6, the series identified by L +, which presents a decrease of conversion, also presents an increase of 14 % in holdup and increase of 80 % in LHSV, which implies a decrease of 50 % in liquid residence time. The series identified by L− exhibits an increase in conversion 222 %, shows decreases of 33 % of liquid holdup, and 500 % in LHSV, which implies an increase of 500 % in residence time of the liquid phase.

As seen in the table included in Figure 6, the increase or decrease of the conversion for HDS and HDN reactions is directly related to the increase or decrease of the residence time of the liquid and gas phases (the longer the residence time, the greater the conversion), while the significance of the changes in the conversion is strongly determined by the magnitude of the variation of the liquid holdup.

Figure 7 shows the effect of temperature and pressure over sulphurized and nitrated species concentration along the reactor length. Figure 7a shows, for the case of T = 653.15, that at higher pressures the conversions for the nitrated and sulphurized species are also higher. It is important to point out that the effect of the pressure is considered in the properties of the fluids (p, μ), the Henry's constant for each species (H_i), which has an important effect in the resistance to the transfer between the gas and liquid phases (see the Mass Transport Model Section) and in the pressure field along the reactor length.

As can be seen from Figure 7a, a decrease of 12 % in operating pressure (from 10–8.8 MPa) leads to a decrease of 7.22 and 17.18 % in the conversion of the sulphurated and nitrated species, respectively. A 35 % decrease in operating pressure (from 10–6.5 MPa) leads to decreases of 22 and 39 % in the same conversions. Figure 7b shows similar information to Figure 6a, but the temperature of operation is 633.15 K. In this case, the decreases of 12 and 35 % in the operating pressure lead to a decrease in 0.84 % (RS), 7.17 % (RN), 15.4 % (RS), and 34.36 % (RN), for RS and RN species conversion for both pressure operations, respectively. Finally, Figure 7c shows, for T = 623.15 cases, the same decrease in pressure leads to a reduction of the conversions of the sulphurized and nitrated species by 12.12 and 22.61 % for a decrease of 12 % in the operation pressure as well as 11 and 30 % for the decrease of the 35 % in operation pressure.

A similar discussion can be made on the effect of decreasing or increasing the temperature. Tables 6 and 7 show a summary of the results obtained.

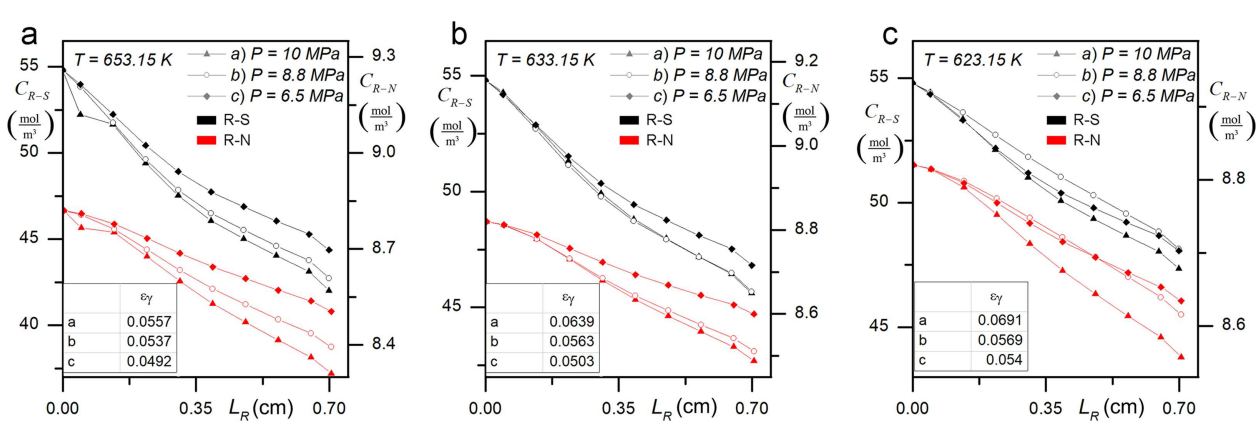

Figure 7. (a) Effect of the temperature and the operation pressure over the *R-S* and *R-N* average concentration fields along the reactor, T = 653.15 K; (b) effect of the temperature and the operation pressure over the *R-S* and *R-N* average concentration fields along the reactor, T = 633.15 K; and (c) effect of the temperature and the operation pressure over the *R-S* and *R-N* average concentration fields along the reactor, T = 623.15 K.

Table 6. Effect of the decrease in the operation pressure at different temperatures over the sulphurated and nitrated species conversion, in reference to the P = 10 MPa cases

		T (*K*)					
		623.15		633.15		653.15	
P (MPa)	ΔP (%)	ΔX_{RS} (%)	ΔX_{RN} (%)	ΔX_{RS} (%)	ΔX_{RN} (%)	ΔX_{RS} (%)	ΔX_{RN} (%)
10	0	0	0	0	0	0	0
8.8	−12	−12.12	−22.61	−0.84	−7.17	−7.22	−17.18
6.5	−35	−11.07	−30.01	−15.4	−34.36	−22.74	−39.6

(Deviation percentages are calculated for each temperature in reference to the P = 10 MPa case)

Table 7. Effect of the increase in the operation temperature at different pressures over the sulphurated and nitrated species conversion, in reference to the T = 653.15 K cases

		P (MPa)					
		10		8.8		6.5	
T (*K*)	ΔK (%)	ΔX_{RS} (%)	ΔX_{RN} (%)	ΔX_{RS} (%)	ΔX_{RN} (%)	ΔX_{RS} (%)	ΔX_{RN} (%)
653.15	0	0	0	0	0	0	0
633.15	−1.6	−33.8	+10.5	−29.29	−28.6	−27.54	−30.77
623.15	−4.8	−48.2	+42.8	−51	−53.1	−40.4	−41.9

(Deviation percentages are calculated for each pressure in reference to the T = 653.15 K case)

In general, it is well known that at higher pressures the solubility of hydrogen increases and at higher temperatures the reaction rate increases, so it is expected that the conversion of both sulphurated and nitrated species increases; this behaviour is evident in Figure 7a. However, in Figure 7b, the series corresponding to 10 and 8.8 MPa are close and even show crossings along the reactor. In Figure 7c, an atypical behaviour is shown because the conversion at 6.5 MPa is greater than at 8.8 MPa. This is a consequence of the highly non-linear interdependence between the pressure, the temperature with the properties of the fluids (gas and liquid), the mass exchange between the gas and liquid phases, the reaction rate, and the hydrodynamics of the reactor.

The possible explanation for these atypical behaviours can be sought through a detailed analysis of the characteristics of the mass transport, the interfacial resistances for the mass transport, and the convective and diffusive fluxes of mass at a local level in the particular length of the reactor where these anomalies occur; this analysis will be part of our future work.

Figure 8 shows the effect of liquid holdup over R-S and R-N species conversion. The figure shows two sets of data: 1) a series of conversion data corresponding to changes in the liquid holdup due to changes in the feed rates of the gas and liquid phases (series with empty circles); and 2) conversion data series corresponding to changes of liquid holdup due to changes in temperature and pressure (series with full diamonds). The data that corresponds only to the changes in the velocities of gas and liquid phases show a clear trend (dashed lines) and shows that at lower liquid holdup, the higher conversions of both species (R-S and R-N) are obtained in the HDS reactor. On the other hand, the conversion data that corresponds to changes in liquid holdup due to the changes in temperature and pressure operation conditions (the same cases shown in Figure 7a to 7c) exhibit a very different behaviour.

It is worth mentioning that the series with empty circles reflect the effect of hydrodynamic changes, through liquid holdup, over the conversion of both R-S and R-N species. The series with diamonds shape marker, on the other hand, reflect the effect of changes in the hydrodynamics, the reaction rate, and the conditions of the solubility of the hydrogen and sulfuric acid (all at the same time) due to temperature and operation pressure changes (over the conversion of R-S and R-N). Consequently, it can be inferred that the model that considers the coupling between hydrodynamics and transport-reaction leads to substantially different results from models that do not. In addition, it can be inferred that reactor models that disregard hydrodynamics can lead to significant deviations in the prediction of conversions because they have to appeal to assumptions and idealizations such

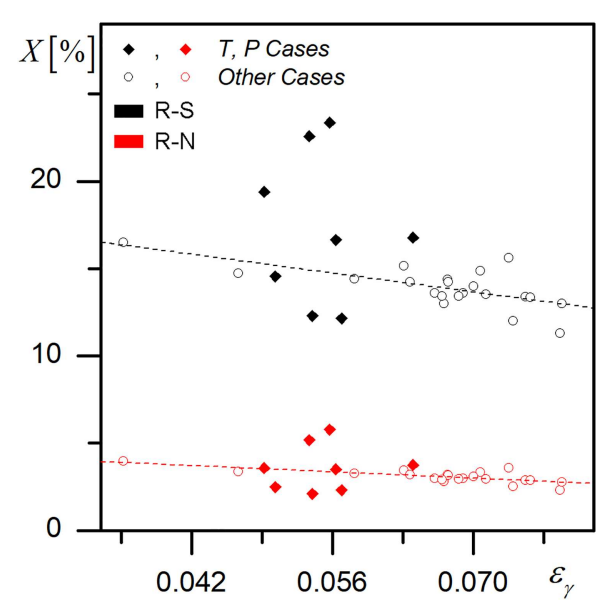

Figure 8. *R-S* and *R-N* species average outlet conversion at different holdups.

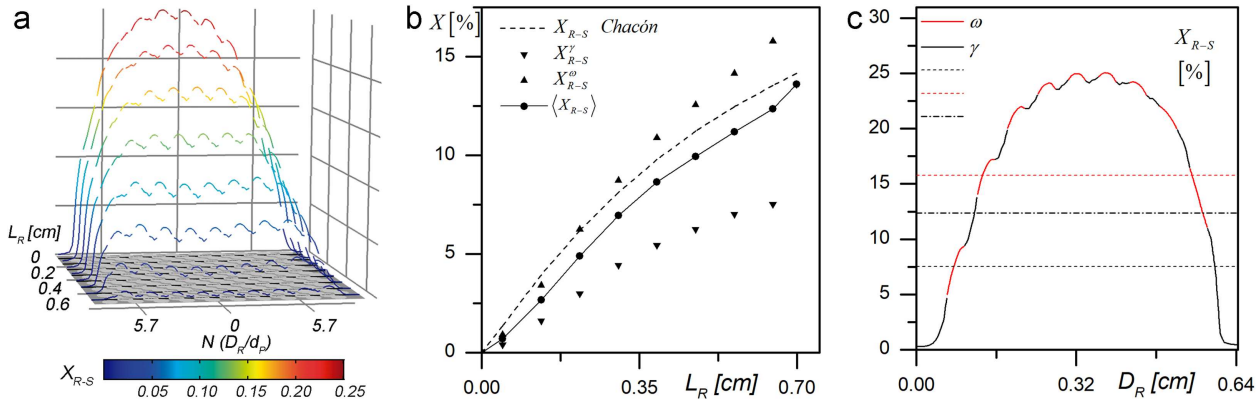

Figure 9. a. Variation of *R-S* species conversion at reactor diameter along the reactor length; b. Variation of the average *R-S* species conversion in the liquid and solid phase, and liquid-solid average conversion; c. Comparison between punctual, solid and liquid cut-plane average and liquid-solid average conversion of *R-S* species.

as plug flow, which can lead to considerable deviations from hydrodynamic and kinetic real behaviour (as will be discussed in the results shown in Figure 9).

Since in the CFD model implemented here the three phases of the HDS reactor are distinguished, it is possible to evaluate the concentration of the sulphurated and nitrated species in the liquid and solid pseudo-phases and to observe the differences in the transport of such species between those phases. The differences in transport are attributed to the differences in the properties of the phases and the fact that the reaction only occurs in the solid pseudo-phase. Furthermore, since the CFD model also explicitly describes the distribution of the catalysts and, therefore, the porosity distribution, it is possible to determine the effect of this distribution on the concentration and conversion fields both along the length of the reactor and in the radius of the reactor.

Figures 9a–c are an exemplification of the information mentioned above. Figure 9a shows the variation of sulphurated species conversion along the reactor diameter and length and explicitly shows the field differences between the liquid phase (sink) and the solid phase (summit) conversion field. On the other hand, Figure 9b shows the variation along the reactor length of radial average conversion considering liquid (X^{γ}_{R-S}) and solid (X^{ω}_{R-S}) phases and considering both phases $\langle\langle X_{R-S}\rangle\rangle$. For comparison purposes, the data of Chacón et al. is also shown.

Finally, Figure 9c shows a comparison between punctual/local, solid and liquid cut-plane average, and liquid-solid average conversion of R-S species and highlights the differences between the averages in solid (−17 %) and liquid (−44 %) domain from the average in both domains. Figure 9c also shows a wall effect in a region, corresponding to 1.5 catalyst diameters, and shows that

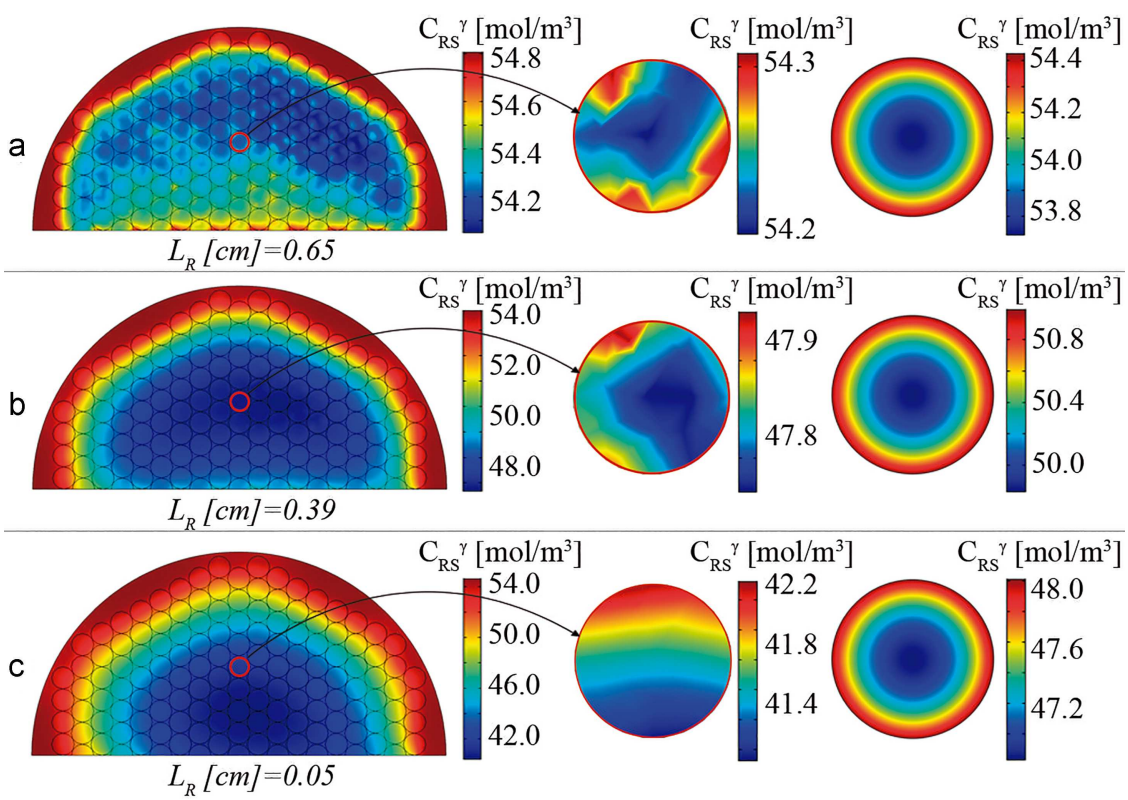

Figure 10. Comparison between the predicted results by the fully coupled model and the isolated catalytic particle model.

this region does not suffer significant variations throughout the reactor.

Another important observation about Figure 9c is that the model exhibits important radial variations of the conversion (and of the concentration) and, thus, the assumption of a plug flow model, in which radial variations are considered as negligible is not satisfied. In this regard, the TBR model for the HDS process that is implemented here corresponds to an experimental isothermal reactor used to determine kinetic expression, for which a plug flow behaviour was considered[32] and its simulation was implemented through a three-phase plug flow reactor model.[33]

The assumptions made in the cited work above are commonly assumed and found in literature for this kind of system; however, it is common to find only brief qualitative justifications for such an assumption.[52] Modern tools as CFD allow researchers to quantitatively confirm or deny the validity of this assumption. For the present case of study, the validity of the plug flow assumption does not seem to be satisfactory.

Figure 10 shows the R-S species concentration field at three cut planes located along reactor length. Figure 10 also shows the same concentration field for a catalytic particle in those cut planes, which is indicated in the cut plane in the figure. Figure 10 shows R-S species concentration fields in a catalytic particle, obtained by solving the mass transport equations with reaction on an isolated catalytic particle scale. In this model, it is considered that the concentration at the pellet surface is equal to the average concentration in the corresponding cut plane, which implies that the interaction with the reactor behaviour is not considered.

In Figure 10, it can be seen that for the three cut planes there are radial gradients of concentration, which implies that the assumption of the plug-flow model is not satisfied. A non-homogeneous distribution of concentration fields and the process of homogenization can also be seen throughout the reactor length. For the present study, it was found that 19 d_P are required to achieve said homogenization while the literature suggests that for these kinds of systems over 30 d_P are required.[53]

Finally, the differences between the concentration fields of the isolated catalytic particles models and the models that consider the interactions and exchange of information with the reactor-scale transport phenomena are contrasted. It is important to note that the models that consider the isolated catalytic particle and, thus, that do not consider the transport phenomena of the reactor, produce symmetric concentration fields and substantially higher conversions than the particles that are embedded in the catalytic reactor. Furthermore, these kinds of isolated models, which predict symmetric fields, are used to evaluate the effectiveness factor even though their predictions are distant from the multiscale-coupled models. These last particles also exhibit a fairly asymmetrical behaviour, that has not been reported in the literature. The explanation for these observed phenomena requires the local analysis of concentration and velocity fields as well as mass diffusive and convective fluxes between the gas, liquid, and solid phases; however, this analysis will be presented in a later work.

CONCLUSIONS

Regarding to the CFD model, it is important to highlight that the proposed model is one of the few models that properly incorporates a rigorous description of the fluid-solid interface areas and distribution of the void fraction (in which the momentum interchange of the hydrodynamics of two-fluid phases interacting with a solid phase is coupled with the mass transport for a hydrotreating process) and that also considers simultaneous HDS and HDN reactions of a light gas oil (LGO). The model involves 13 mass transport equations for the species R-S, R-N, H_2, H_2S, and NH_3, 2 momentum balance equations, and 3 closures to take into account the liquid-solid, liquid-gas, and gas-solid interactions.

The hydrodynamic model results show a substantial improvement in the prediction of pressure drop (5 times better accuracy) and liquid holdup (50 % improvement) at high and low operation pressure, compared with experimental data. Also, the hydrodynamics and mass transfer coupled model leads to predictions of the HDS and HDN conversions in agreement with the reported results found in literature. The deviation in the prediction of the outlet conversions are of up to 4.7 % for the sulphurated species and 5.5 % for the nitrated species. Thus, the proposed CFD model exhibits an excellent predictive capability for both hydrodynamic and kinetic behaviours.

An analysis involving four ways of comparing columns with different diameter and length were presented. The results show that equaling the holdups of both columns leads to similar pressure drops and conversion values for both columns. These results could mean a remarkable finding that eventually allows the establishing of scaling techniques based on a more scientific basis; however, it is still desirable to analyze and compare several reactors of different dimensions and involve different processes that lead to more conclusive results.

It is known that the geometry of the microstructure and the mass transport inside the pores of the catalyst exerts an effect on the overall behaviour of the reactor; however, until now, this relationship had not been quantified. In the present study, a quantitative analysis of multiscale phenomena that analyzes the effect of microstructure geometry and mass transport at microstructure catalyst over the reactor behaviour was developed. It was found that the effect could be considerable and that variations of up to 38 % in the evaluation of the effective diffusivity can lead to differences of 30 % in the prediction of the kinetic behaviour inside the reactor. This implies that the overall behaviour of the reactor is actually sensitive to the textural changes of the representation of the pores microstructure. Therefore, models that neglect the coupling between scales might have over-simplifications that can lead to important deviations in their predictions.

In the proposed CFD model, a multiscale analysis was developed involving the pore microstructure, catalytic particle, and reactor scales. The model considers the transport of information at the pore level towards the catalytic pellet and reactor scales and the transport of information in two directions between the pellet and reactor scale, which differs from models commonly found in literature that only consider the transport of information in one direction.

Aided by the proposed model, which has proven its predictive capability, further analysis to determine the effect of operating conditions (variation in feed rates of gas and liquid streams as well as temperature and pressure) on the conversions achieved in the HDS reactor were performed. Similar studies can be found in the literature for several cuts of crude oil; however, in most of them, a constant and average value of the holdup, pressure, and velocity of phases has been assumed. This implies that the effect of the hydrodynamics inside the reactor on the kinetic-mass behaviour of the reactor is neglected. In contrast, in the model implemented here, the effect of variation of operation conditions is incorporated through fluid properties such as density and viscosity as well as hydrodynamics parameters such as liquid holdup and pressure drop; therefore, the combined effect of all these parameters on the conversion in the reactor was quantified. Consequently, the effect

of operation conditions was considered in both hydrodynamics and mass transport with reaction phenomena, and the results show that there are differences in the prediction for conversion in HDS reactor when the effect of the operation conditions on the hydrodynamics is neglected or not.

In the CFD model implemented in this work, an analysis of the assumptions of the plug flow was developed. The results show that there are radial gradients of concentration and, consequently, considerable deviations to the typical assumption of plug flow regime, so that the descriptive justifications found in the literature regarding the validity or otherwise of the plug flow could be inadequate or unreliable. Moreover, the coupling of mass transport with a consideration of the interaction between pellet scale transport phenomena with reactor scale phenomena leads to substantially different or unpredicted results from those in which both scales are analyzed independently. Furthermore, the model coupling the multiscale show atypical tendencies that had not been predicted by the models found in literature. Further analysis regarding the local scale phenomena at the different length scales is required in order to understand the observed behaviours.

NOMENCLATURE

Symbols

a_s	Pellet specific area (m^{-1})
a_v	Catalyst microstructure specific area (m^{-1})
$A_{j\omega}$	Solid-fluid interphase (m^2)
$\mathbf{b}_\lambda$	Closure vector for mass transport problem
C_i^π	Concentration of species i in π-phase ($mol\ m^{-3}$)
$\tilde{C}_i^\pi$	Concentration deviation of species i in π-phase ($mol\ m^{-3}$)
$\langle C_i^\pi \rangle$	Average concentration of species i in phase π ($mol\ m^{-3}$)
D_i^j	Diffusivity of species i in j-phase ($m^2\ s^{-1}$)
$D_{eff,i}$	Effective diffusivity of species i of fluid phase ($m^2\ s^{-1}$)
$\mathbf{D}_{eff,i}^\omega$	Effective diffusivity of species i in catalyst pseudo-phase ($m^2\ s^{-1}$)
d_p	Pellet diameter (m)
D_R	Reactor diameter (m)
ΔH_{HDS}	Heat of reaction ($J\ mol^{-1}$)
$E_{a,j}$	j reaction activation energy ($J\ mol^{-1}$)
E_1	First Ergun constant
E_2	Second Ergun constant
$\mathbf{F}_i$	Interaction force term ($N\ m^{-3)}$
$\mathbf{g}$	Gravitational constant ($m\ s^{-2}$)
G	Gas mass flow ($kg\ m^{-2}\ s^{-1}$)
H_i	Henry coefficient for species i ($m^3\ Pa\ mol^{-1}$)
k_{HDS}	Pre-exponential factor for HDS reaction $\left(\left(\frac{m^3}{mol}\right)^{0.5} s^{-1}\right)$
k_{HDN}	Pre-exponential factor for HDN reaction ($m^3\ mol^{-1}\ s^{-1}$)
k_i^0	Pre-exponential factor for adsorption of i species ($m^3\ mol^{-1}$)
K_i	Species i adsorption constant ($mol\ m^{-3}$)
$K_{g,i}^{\beta\gamma}$	Gas-liquid mass transfer coefficient for species i (s^{-1})
$K_i^{\gamma\omega}$	Liquid-solid mass transfer coefficient for species i ($m\ s^{-1}$)
K_{kj}	Momentum exchange coefficient between k and j phases ($kg\ m^{-3}\ s^{-1}$)
L	Liquid mass flow ($kg\ m^{-2}\ s^{-1}$)
L_R	Reactor length (m)
$\mathbf{I}$	Identity matrix
$MW_{gas\ oil}$	Gasoil molecular weight ($g\ mol^{-1}$)
$N_i^{\beta\gamma}$	Volumetric mass exchange of species i between gas and liquid phases ($mol\ m^{-3}s^{-1}$)
$\mathbf{N}_i^j$	Total molar flux of species i ($mol\ m^{-2}s^{-1}$)
$-\mathbf{n}$	Unitary normal vector
N	Reactor to pellet diameter ratio
N_c	Critical reactor to pellet diameter ratio
P	Pressure (Pa)
Q_i	Species i adsorption energy ($J\ mol^{-1}$)
$\langle r_q^\omega \rangle^\omega$	Average reaction rate for q reaction ($mol\ m^{-3}\ s^{-1}$)
R_g	Constant of ideal gases ($J\ mol^{-1}\ K$)
Re^i	Reynolds number for phase i
T	Temperature (K)
$\mathbf{v}_j$	j phase local interstitial velocity ($m\ s^{-1}$)
$(\mathbf{v}_j - \mathbf{v}_i)$	slip velocity between j and i phases ($m\ s^{-1}$)
V_j^0	j phase inlet velocity ($m\ s^{-1}$)
X_i	Conversion for i-reaction
ΔP	Pressure drop (Pa)

Greek Symbols

β	Ga phase
γ	Liquid phase
ω	Solid pseudo-phase
ε_i	i phase volume fraction
ε_γ	Liquid holdup
ε_σ	Pellet porosity
ε_B	Bed porosity
μ_i	Species i dynamic viscosity ($Pa\ s$)
λ	fluid phase in catalyst
ρ_i	Species i density ($kg\ m^{-3}$)
σ	Solid phase in catalyst
v_i	Species i stochiometric coefficient
Ψ	Dimensionless pressure drop

Sub and Superscripts

0	Initial conditions
op	Operation conditions

Abbreviations

GHSV	Gas hourly space velocity (s^{-1})
LHSV	Liquid hourly space velocity (s^{-1})
LHHW	Langmuir-Hinshelwood/Hagen-Watson kinetics
MARE	Mean absolute relative error
IMEM	Interphase momentum exchange model
RUC	Representative Unitary Cell
CC	Quadrangular Centered (RUC)
CA	Quadrangular Alternated (RUC)
RA	Rectangular Alternated (RUC)
RM	Realistic Model
CFD	Computational Fluid Dynamics
TBR	Trickle Bed Reactor
EXP	Experimental value
CALC	Calculated value with CFD model
HDA	Hydrodearomatization
HDS	Hydrodesulphurization

HDN	Hydrodenitrogenation
$R-S$	Sulphurized species
$R-N$	Nitrated species
H_2S	Hydrogen sulfide
NH_3	Ammonia
N_2	Nitrogen
H_2	Hydrogen

REFERENCES

[1] P. Schacht, S. Ramírez, J. Ancheyta, *Energ. Fuel*. **2009**, *23*, 4860.

[2] M. H. Al-Dahhan, M. P. Dudukovic, *Chem. Eng. Sci*. **1995**, *50*, 2377.

[3] D. Lasseux, F. J. T. Valdés-Parada, *C.R. Mecanique* **2017**, *345*, 660.

[4] H. Nadeem, I. B. Salem, M. Sassi, *Chem. Eng. Commun*. **2017**, *204*, 388.

[5] M. Bandari, Y. Behjat, S. Shahhosseini, *Int. J. Chem. React. Eng*. **2012**, *10*, 1.

[6] Z. Solomenko, Y. Haroun, M. Fourati, F. Larachi, C. Boyer, F. Augier, *Chem. Eng. Sci*. **2015**, *126*, 698.

[7] A. Kundu, K. D. P. Nigam, R. P. Verma, *AIChE J*. **2003**, *49*, 2253.

[8] F. Augier, A. Koudil, A. Royon-Lebeaud, L. Muszynski, Q. Yanouri, *Chem. Eng. Sci*. **2010**, *65*, 255.

[9] M. E. Cordero, S. Uribe, L. G. Zárate, R. Natividad-Rangel, A. Regalado-Méndez, E. Peralta-Reyes, *Computational Fluid Dunamics*, InTech Open, Rijeka **2018**.

[10] O. Derkx, A. G. Dixon, *Numer. Heat Tr. A-Appl*. **1996**, *29*, 77.

[11] M. Nijemeisland, A. G. Dixon, *Chem. Eng. J*. **2001**, *82*, 231.

[12] R. J. G Lopes, R. M. Quinta-Ferreira, *Chem. Eng. Sci*. **2009**, *64*, 1806.

[13] K. Lappalainen, M. Manninen, V. Alopaeus, *Chem. Eng. Sci*. **2009**, *64*, 207.

[14] R. K. Reddy, J. B. Joshi, *Particuology* **2010**, *8*, 37.

[15] A. H. Beni, M. R. Khosravi-Nikou, *Pet. Sci. Technol*. **2016**, *3*, 1770.

[16] P. Niegodajew, D. Asendrych, S. Drobniak, *Journal of Power Technologies* **2013**, *93*, 354.

[17] P. Horgue, F. Augier, P. Duru, M. Prat, M. Quintard, *Chem. Eng. Sci*. **2013**, *102*, 335.

[18] M. Bazmi, S. H. Hashemabadi, M. Bayat, *Int. Commun. Heat Mass* **2012**, *39*, 736.

[19] M. Macias, J. Ancheyta, *Catal. Today* **2004**, *98*, 243.

[20] I. Iliuta, F. Larachi, B. P. A. Grandjean, *Ind. Eng. Chem. Res*. **1998**, *37*, 4542.

[21] S. Mitra, *Computational Fluid Dynamics Modeling of Trickle Bed Reactors*, VDM Verlag, Saarbrücken **2011**.

[22] M. E. Cordero, S. Uribe, L. G. Zárate, J. A. Hernandez-Servin, E. Peralta-Reyes, A. Regalado-Méndez, *Int. J. Chem. React. Eng*. **2017**, *15*, 1.

[23] M. H. Al-Dahhan, M. P. Dudukovic, *Chem. Eng. Sci*. **1994**, *49*, 5681.

[24] D. Nemec, J. Levec, *Chem. Eng. Sci*. **2005**, *60*, 6958.

[25] M. E. Trivizadakis, D. Giakoumakis, A. J. A. Karabelas, *Chem. Eng. Sci*. **2006**, *61*, 5534.

[26] M. Bazmi, S. H. Hashemabadi, M. Bayat, *Pet. Sci. Technol*. **2013**, *3*, 21.

[27] F. Augier, F. Idoux, J. Y. Delenne, *Chem. Eng. Sci*. **2010**, *65*, 1055.

[28] S. Afandizadeh, E. A. Foumeny, *Appl. Therm. Eng*. **2001**, *21*, 669.

[29] F. S. Mederos, J. Ancheyta, *Appl. Catal. A-Gen*. **2007**, *332*, 8.

[30] A. Heidari, S. H. Hashemabadi, *Chem. Eng. Res. Des*. **2015**, *94*, 549.

[31] M. Bazmi, S. H. Hashemabadi, M. Bayat, *Int. J. Heat Mass Tran*. **2011**, *38*, 391.

[32] C. Botchwey, A. K. Dalai, J. Adjaye, *Energ. Fuel*. **2003**, *17*, 1372.

[33] R. Chacón, A. Canale, A. Bouza, Y. Sanchez, *Braz. J. Chem. Eng*. **2012**, *29*, 135.

[34] A. O. Silva, C. A. A. Monteiro, V. P. De Souza, A. S. Ferreira, R. P. Jaimes, D. V. R. Fontoura, J. R. Nunhez, *Fuel Process. Technol*. **2017**, *166*, 17.

[35] S. Whitaker, *The Method of Volume Averaging*, Kluwer Academic Publishers, Dordrecht **1999**.

[36] F. Valdés-Parada, D. Lasseux, F. Bellet, *Adv. Water Resour*. **2016**, *90*, 70.

[37] G. Benítez-Olivares, F. J. Valdéz Parada, J. G. Saucedo-Castañerda, *Int. J. Chem. React. Eng*. **2016**, *14*, 1115.

[38] F. Dorai, C. M. Teixeria, M. Rolland, E. Climent, M. Marcoux, A. Wachs, *Chem. Eng. Sci*. **2015**, *129*, 180.

[39] S. T. Sie, *Rev. I. Fr. Petrol*. **1990**, *46*, 501.

[40] N. Ali, T. Al-Juwaya, M. Al-Dahhan, *Particuology* **2017**, *34*, 48.

[41] N. Ali, T. Al-Juwaya, M. Al-Dahhan, *Chem. Eng. Res. Des*. **2016**, *114*, 129.

[42] D. A. Drew, *Annu. Rev. Fluid Mech*. **1983**, *15*, 261.

[43] G. F. Froment, K. B. Bischoff, *Chemical Reactor Analysis and Design*, Wiley, New York **1979**.

[44] M. Auset, A. A. Keller, *Water Resour. Res*. **2004**, *40*, 1.

[45] A. Attou, C. Boyer, G. Ferschneider, *Chem. Eng. Sci*. **1999**, *54*, 785.

[46] R. J. G. Lopes, R. M. Quinta-Ferreira, *Chem. Eng. Sci*. **2010**, *65*, 291.

[47] R. J. G. Lopes, R. M. Quinta-Ferreira, *Chem. Eng. Sci*. **2010**, *160*, 293.

[48] M. E. Cordero, R. Natividad, L. G. Zárate, J. A. Hernandez-Servin, J. Salas, *Catal. Today* **2014**, *220*, 113.

[49] F. Larachi, A. Laurent, N. Midoux, G. Wild, *Chem. Eng. Sci*. **1991**, *46*, 1233.

[50] S. Goto, J. M. Smith, *AIChE J*. **1975**, *21*, 706.

[51] V. Speccia, G. Baldi, A. Gianetto, *Ind. Eng. Chem. Proc. D.D*. **1978**, *17*, 362.

[52] F. L. Dryer, F. M. Haas, J. Santner, T. I. Farouk, M. Chaos, *Prog. Energ. Combust*. **2014**, *44*, 19.

[53] D. E. Mears, *Chem. Eng. Sci*. **1971**, *26*, 1361.

Manuscript received January 15, 2018; revised manuscript received April 20, 2018; accepted for publication May 22, 2018.